Shell formation in short like-charged polyelectrolytes in a harmonic trap

Sandipan Dutta[1] and Y. S. Jho[1,2,*]
[1]*Asia Pacific Center for Theoretical Physics, Pohang, Gyeongbuk, 790-784, Korea*
[2]*Department of Physics, Pohang University of Science and Technology, 790-784, Korea*
(Received 24 September 2015; published 27 January 2016)

Inspired by recent experiments and simulations on pattern formation in biomolecules by optical tweezers, a theoretical description based on the reference interaction site model (RISM) is developed to calculate the equilibrium density profiles of small polyelectrolytes in an external potential. The formalism is applied to the specific case of a finite number of Gaussian and rodlike polyelectrolytes trapped in a harmonic potential. The density profiles of the polyelectrolytes are studied over a range of lengths and numbers of polyelectrolytes in the trap, and the strength of the trap potential. For smaller polymers we recover the results for point charges. In the mean field limit the longer polymers, unlike point charges, form a shell at the boundary layer. When the interpolymer correlations are included, the density profiles of the polymers show sharp shells even at weaker trap strengths. The implications of these results are discussed.

DOI: 10.1103/PhysRevE.93.012503

I. INTRODUCTION

Optical tweezers are excellent tools to trap and manipulate colloidal particles [1]. Focusing an intense laser beam into a colloidal solution of nanoparticles [2–5] or polymers [6–8] generates a field gradient which can cause their aggregation. Due to this capability, it serves as a principal technique for controlled two- and three-dimensional (2D and 3D) pattern formations in biomolecules which has applications in optical sorting of biological systems, cells micromachines, and manipulation of biopolymers [9–12]. In recent experiments the polymers have been deposited on a 2D substrate by laser beams [6,13]. The formation of microstructures in flexible biomolecules on metallic nanostructures has provided a mechanism for their application in the development of biosensors [14,15]. These biopolymers form ring structures under the laser radiation forces. Such kinds of pattern formations have also been observed in trapped liquid crystals [16–19] and in point-particle plasmas [20–23]. The pattern formations in the trapped systems are often a result of competing effects of the repulsive interactions, such as electrostatic or hydrophobic interactions and the trap potential, causing reversible phase transitions in polymer gels [24] or the shell structure in plasmas. Many biomolecules, for instance, the rodlike virus or liquid crystals or the helical DNA or RNA molecules, have finite sizes and their geometries play a critical role in the formation of these patterns [9–11,18,19]. It is very important to understand how the finite-sized particles behave in the trapping potential of the optical tweezers. While the theoretical and simulation studies on trapped point-charges are extensive [25–33], very few theories exist for finite-sized charges in traps. The objective of this work is to theoretically study the distribution of charged polymers in a trap potential to understand the underlying mechanisms of the structure formation in charged biomolecules. In many colloidal and plasma systems, the pattern formation is due to the presence of some short-ranged attractive forces in the system [34–40]. Here we show that the pattern formations can occur even in the absence of the attractive interactions, primarily due to the competing effects of the trap and the electrostatic repulsions.

In many optical traps the trapping potential can be well approximated by a harmonic well [41,42]; hence in this work we specialize to the case of harmonic traps. Wrighton *et al.* have developed a theory, based on classical density functional theory (DFT) and hypernetted chain approximation (HNC), to study the shell formation in a system of finite number of point charges in a harmonic trap [25–27]. They found that strong correlations are essential to the formation of shells they successfully predict the location, number, and filling of the shells. The extension of their theory to polymers is not straightforward because of the additional orientational degrees of freedom, constraints of connectivity, and finite size of the polymers. Additionally, in the case of polymers, due to their finite sizes, intrapolymer correlations have to be taken into account together with the interpolymer correlations. The reference interaction site model (RISM) by Chandler *et al.* provides a tool to calculate the density profile of the polymers in the presence of an external potential and include both kinds of correlations [43,44]. In this formalism the equilibrium density at each site of a polymer is a functional of the external potential and correlations at that site. This approach, however, is not very convenient, as a coupled set of nonlinear equations corresponding to each site needs to be solved to obtain the density profile at each site. For uniform polymer systems, Schweizer and Curro [45–47] have developed a theory by averaging over the sites of the polymers, popularly known as the polymer reference interaction site model (PRISM). The PRISM theory has been successfully applied to a variety of polymer systems, including polymer crystallization, symmetric as well as asymmetric polymer blends, and block copolymers. In the spirit of the PRISM formalism, we compute the average equilibrium polymer density in nonuniform systems by replacing the site quantities by their corresponding site averages. This vastly reduces the complexity of the problem of solving matrix equations in the RISM formalism. As a result of this we obtain a single equation

*ysjho@apctp.org

for the site-averaged density of the polymers as a function of the site-averaged correlations and external potential.

The outline of the paper is as follows. In Sec. II we phenomenologically derive an integral equation for the equilibrium site-averaged density of polymer in an external potential based on the RISM formalism. From this equation we obtain a closure relation to the PRISM equation similar to the one obtained by Laria, Wu, and Chandler (LWC) for the pair correlation functions [48], which is the molecular equivalent of the HNC equation. In the limit of small polymer length we recover the HNC equation for the point-particle density. We apply our formalism to the specific case of finite number of polyelectrolytes trapped in a harmonic potential. We derive the density profiles of Gaussian polyelectrolytes in the mean field approximation in Sec. III. The polymer-polymer correlations are calculated using the LWC and PRISM equations in Sec. IV. We go beyond the mean field approximation and obtain the monomer densities with the full many-body correlations. The dependence of the correlated densities on the geometry of the polyelectrolytes and the strength of the trap potential are worked out. In Sec. V we briefly look into the density profiles of rodlike polyelectrolytes and compare them with the Gaussian polyelectrolytes to investigate dependence of the shell formation on the polymer model. We discuss the limitations of the averaging procedure and the range of validity of our model in Sec. VI.

II. THE FORMALISM

Consider a system of N polyelectrolytes each consisting of L monomers. Each monomer has a length σ and charge q. For simplicity we assume the hard core diameter of the polymers equals the monomer length σ. Thus the length and charge of each polymer would be $L\sigma$ and Lq, respectively. The polymers are confined by a harmonic potential of the form $\phi(\mathbf{r}) = \frac{1}{2}Kr^2$. The schematic diagram of the system is shown in Fig 1. The electrostatic interactions between polymers has a Coulomb form $V(|\mathbf{r}-\mathbf{r}'|) = 1/|\mathbf{r}-\mathbf{r}'|$. The coordinate of the polymers at segment s is parameterized by a field $\mathbf{x}(s)$. The Hamiltonian of the system reads

$$H = \sum_{i=1}^{N}\int_0^L ds\phi[\mathbf{x}_i(s)] + \frac{q^2}{2\epsilon}\sum_{i\neq j}\int_0^L ds\int_0^L ds' V[|\mathbf{x}_i(s)-\mathbf{x}_j(s')|], \quad (1)$$

where ϵ is the dielectric constant of the medium. The average intermonomer distance r_0 is related to the average monomer density $\bar{\rho}$ by $\frac{4\pi}{3}r_0^3\bar{\rho} = 1$. If R is the size of the trap (the position of the outermost polymer in the trap), then the average monomer density is given by $\bar{\rho} = \frac{NL}{(4\pi/3)R^3}$. R can be approximately obtained from the position of the outermost polymer such that the average forces on it would be zero, $\frac{1}{\epsilon R^2}q^2LN = KR$ [25]. We define the dimensionless distance by $\mathbf{r}^* = \mathbf{r}/r_0$ and the dimensionless polymer segment field by $\mathbf{x}^*(s) = \mathbf{x}(s)/r_0$. The dimensionless monomer length is defined in a similar way, $\sigma^* = \sigma/r_0$. The dimensionless total

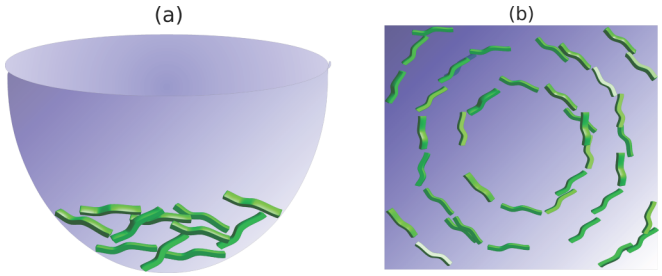

FIG. 1. (a) Schematic diagram showing polyelectrolytes trapped in a harmonic trap. (b) Concentric ringlike structures form due to the competing effects of the trap force and the electrostatic forces in 2D. In 3D (not shown) concentric shells are formed.

potential is given by

$$\beta V = \frac{\Gamma}{2}\left[\sum_{i=1}^{N}\int_0^L ds x_i^{*2}(s) + \sum_{i\neq j}^{N}\int_0^L ds\int_0^L ds'\frac{1}{|\mathbf{x}_i^*(s)-\mathbf{x}_j^*(s')|}\right], \quad (2)$$

where the inverse thermal energy is $\beta = 1/k_BT$ and $\Gamma = \beta q^2/\epsilon r_0$ is the strength of the Coulomb interactions among two monomers. The thermodynamic parameter Γ measures the strength of the Coulomb potential between the monomers relative to the kinetic or thermal energy k_BT. For a given trap strength K, if some polymers are dropped into the trap they would come to equilibrium such that the electrostatic repulsions are balanced by the trap potential. Since Γ is determined in terms of the average intermonomer distance, which is obtained from the force balance condition, K and Γ are not independent. In fact, they are the same in the special case when the distances are scaled with respect to r_0 and the trap is harmonic, as we see in Eq. (2). From now on we use Γ for the strength of the trap.

We relate the potential to the density of the polymers through the RISM formalism developed by Chandler *et al* [44]. In the rest of the discussions we use only the dimensionless quantities and to keep their notations simple we drop $*$. The density at site $\alpha, \rho_\alpha(\mathbf{r})$ can be expressed in terms of the intramolecular pair correlation function $\omega_{\alpha\beta}(|\mathbf{r}-\mathbf{r}'|)$, the local chemical potential $\psi_\alpha(\mathbf{r}) = \mu_\alpha - \phi_\alpha(\mathbf{r})$, and the direct correlation function $c_{\alpha\beta}(|\mathbf{r}-\mathbf{r}'|)$:

$$\rho_\alpha(\mathbf{r}) = \prod_{\gamma\neq\alpha}\omega_{\alpha\gamma} * \exp(f_\gamma), \quad (3)$$

where

$$f_\gamma = \psi_\gamma + \sum_\eta c_{\gamma\eta} * \rho_\eta. \quad (4)$$

(Note that we use the direct correlation function of a uniform system for simplicity.) We use the symbol $*$ for the convolution operation $p * q = \int d\mathbf{r}' p(\mathbf{r})q(|\mathbf{r}-\mathbf{r}'|)$ and have dropped the position dependence to keep notations simple. Like the PRISM theory [45,47], we replace the quantities at each site by the corresponding site-averaged quantity. This simplifies the

algebra of Eq. (3) considerably. Summing over the index α and replacing $\omega_{\alpha\gamma}$ by $\omega = \frac{1}{L}\sum_{\alpha\gamma}\omega_{\alpha\gamma}$, we get

$$\rho = \sum_{\alpha}\rho_{\alpha} \approx \prod_{\gamma}\omega * \exp(f_{\gamma}). \tag{5}$$

Chandler proposed an additional convolution on the right-hand side of Eq. (3) with the single polymer site-site pair correlations $\omega_{\alpha\beta}$ for polyatomic systems. Here we convolute with the site-averaged pair correlations instead [44]:

$$\ln\rho \approx \sum_{\gamma}\ln\left[\omega * \exp(f_{\gamma}) * \omega/L\right]. \tag{6}$$

Expanding the exponential on the right-hand side of the above equation until the first-order term we get

$$\begin{aligned}\ln\rho &\approx \sum_{\gamma}\ln(1+\omega * f_{\gamma} * \omega/L)\\ &\approx \omega * \sum_{\gamma} f_{\gamma} * \omega/L\\ &= \omega * f * \omega/L.\end{aligned} \tag{7}$$

Using the explicit form of f in Eq. (4) the final expression of the equilibrium density becomes

$$\ln\rho = \omega * \psi * \omega + \omega * c * \rho * \omega/L, \tag{8}$$

where $\psi = \sum_{\alpha}\psi_{\alpha}$ and $\rho = \sum_{\alpha}\rho_{\alpha}$. This is the equation for the monomer density in terms of the local chemical potential. When one of the polymers is fixed at the origin, it would act as source of the external potential. In this case $\phi(r) = V(r)$ and density in Eq. (8) becomes the pair correlation function between the polymers, $\rho(r) = \bar{\rho}g(r)$ [49]:

$$\ln g = \omega * (-\beta V) * \omega + \bar{\rho}\omega * c * (g-1) * \omega/L. \tag{9}$$

Using the PRISM equation [47]

$$g - 1 = \omega * c * \omega + \bar{\rho}\omega * c * (g-1), \tag{10}$$

we see that Eq. (9) is identical to the HNC formalism of Laria, Wu, and Chandler (LWC) [48] for molecular systems, except for an extra convolution of ω in the second term on the right-hand side. If we put the distance dependence in Eq. (8) and use the external potential instead of the local chemical potential, we get the relation between the monomer density and the external potential,

$$\ln[\rho(\mathbf{r})\lambda^3/z] = -\int d\mathbf{r}'d\mathbf{r}''\omega(|\mathbf{r}-\mathbf{r}'|)\beta\phi(|\mathbf{r}'-\mathbf{r}''|)\omega(r'') + \int d\mathbf{r}'d\mathbf{r}''d\mathbf{r}'''\omega(|\mathbf{r}-\mathbf{r}'|)c(|\mathbf{r}'-\mathbf{r}''|)\rho(|\mathbf{r}''-\mathbf{r}'''|)\omega(r''')/L, \tag{11}$$

where $\lambda = \sqrt{h^2/2\pi m k_B T}$ is the thermal wavelength and z is the fugacity of the system. The direct correlation function $c(|\mathbf{r}-\mathbf{r}'|)$ in the above equation is calculated using the LWC equation [48],

$$\ln g(r) = -\int d\mathbf{r}'d\mathbf{r}''\omega(|\mathbf{r}-\mathbf{r}'|)\beta V(|\mathbf{r}'-\mathbf{r}''|)\omega(r'') + h(r) - \int d\mathbf{r}'d\mathbf{r}''\omega(|\mathbf{r}-\mathbf{r}'|)c(|\mathbf{r}'-\mathbf{r}''|)\omega(r''), \tag{12}$$

and the PRISM equation,

$$g(r) - 1 = \int d\mathbf{r}'d\mathbf{r}''\omega(|\mathbf{r}-\mathbf{r}'|)c(|\mathbf{r}'-\mathbf{r}''|)\omega(r'') + \int d\mathbf{r}'d\mathbf{r}''\omega(|\mathbf{r}-\mathbf{r}'|)c(|\mathbf{r}'-\mathbf{r}''|)\bar{\rho}h(r''), \tag{13}$$

where $\bar{\rho} = \frac{1}{V_0}\int d\mathbf{r}\rho(\mathbf{r})$ and $h(r) = g(r) - 1$. V_0 is the volume of the trap.

We can get rid of the unknown fugacity z on the left-hand side of Eq. (11) by imposing the constraint that there are N polymers on average in the system

$$\int d\mathbf{r}\rho(\mathbf{r}) = NL. \tag{14}$$

This gives

$$\rho(\mathbf{r}) = NL\frac{\exp[-\Gamma U(r)]}{\int d\mathbf{r}'\exp[-\Gamma U(r')]}, \tag{15}$$

where

$$\begin{aligned}U(r,\Gamma,N) = &\int d\mathbf{r}'d\mathbf{r}''\omega(|\mathbf{r}-\mathbf{r}'|)\phi(|\mathbf{r}'-\mathbf{r}''|)\omega(r'') + \frac{N}{\int d\mathbf{r}'\exp[-\Gamma U(r')]}\int d\mathbf{r}'d\mathbf{r}''d\mathbf{r}'''\\ &\times\ \omega(|\mathbf{r}-\mathbf{r}'|)\bar{c}(|\mathbf{r}'-\mathbf{r}''|)\exp[-\Gamma U(|\mathbf{r}''-\mathbf{r}'''|)]\omega(r'''),\end{aligned} \tag{16}$$

with the notation $\bar{c}(|\mathbf{r}-\mathbf{r}'|) = -c(|\mathbf{r}-\mathbf{r}'|)/\Gamma$.

In the rest of the sections we demonstrate the above formalism by applying it to the case of Gaussian and rodlike polyelectrolytes in harmonic traps. In the small polymer limit we make connections to the point-particle results obtained by Wrighton *et al.* [25]. We also compare our findings with the existing literature on the pattern formation in colloidal systems.

III. GAUSSIAN POLYELECTROLYTES: MEAN FIELD APPROXIMATION

In this section we focus on the Gaussian polyelectrolytes trapped in a harmonic potential with mean field interactions among the polymers. We calculate their density profiles from Eq. (16) and investigate their dependence on the geometry

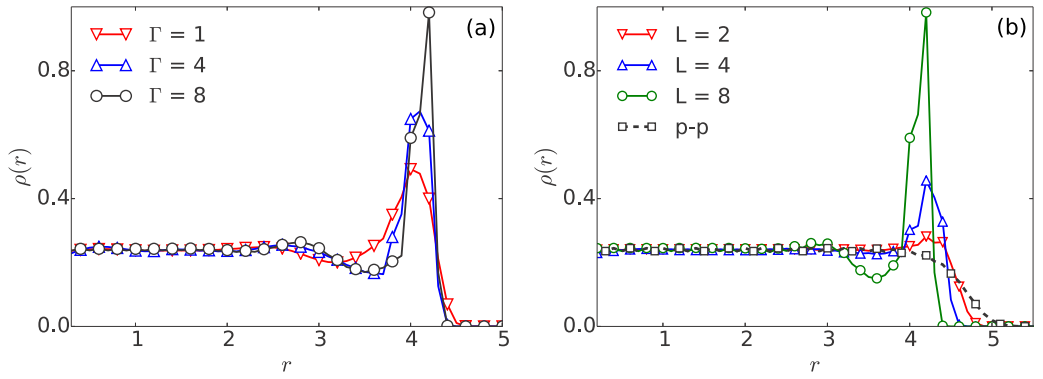

FIG. 2. Mean field. (a) Monomer densities calculated from Eq. (17) for different values of trap strengths Γ for $N = 100$ Gaussian polymers each containing $L = 8$ monomers and monomer length (diameter) $\sigma = 0.5$. Stronger interactions lead to sharper shells. (b) Monomer densities for various lengths L of 100 polymers with $\sigma = 0.5$ and $\Gamma = 8$. Also shown is the point-particle result, p-p. Longer polymers have sharper outermost shells.

of the polymers as well as the strength of the trap (Coulomb coupling parameter) Γ (or the inverse temperature). In the mean field approximation the direct correlation function in Eq. (16) is replaced by the bare interaction potential $-\Gamma/r$:

$$U(r,\Gamma,N) = \frac{1}{2}\int d\mathbf{r}'d\mathbf{r}''\omega(|\mathbf{r}-\mathbf{r}'|)|\mathbf{r}'-\mathbf{r}''|^2\omega(r'') + \frac{N}{\int d\mathbf{r}'\exp[-\Gamma U(r')]}\int d\mathbf{r}'d\mathbf{r}'''\omega(|\mathbf{r}-\mathbf{r}'|) \times\left[\frac{1}{r'}\int_0^{r'} dr''r''^2\exp[-\Gamma U(|\mathbf{r}''-\mathbf{r}'''|)]\omega(r''') + \int_{r'}^{R} dr''r''\exp[-\Gamma U(|\mathbf{r}''-\mathbf{r}'''|)]\omega(r''')\right]. \quad (17)$$

In the limit of point particles, $\omega(|\mathbf{r}-\mathbf{r}'|) = \delta(|\mathbf{r}-\mathbf{r}'|)$, we recover the point-particle mean field equation of Wrighton *et al.* [25].

For Gaussian polymers the single chain structure factor $\hat{\omega}(\mathbf{k})$ in Eqs. (16) and (17) is given by

$$\hat{\omega}(\mathbf{k}) = \left(1 - f^2 - 2f/L + 2f^{L+1}/L\right)/(1-f)^2, \quad (18)$$

where $f = \exp(-k^2\sigma^2/6)$ [47]. The recursive integral equation (17) for $U(r)$ is solved iteratively using the Picard's method [49], and using Eq. (15) we obtain the density. In Fig. 2(a) we plot the monomer densities for the polymers of length $L = 8$ for different strengths of the trap Γ. The dimensionless average monomer density is defined as $\bar{\rho}r_0^3 = 3/4\pi = 0.239$. In Fig. 2 we see that the polymers close to the center of the trap have a uniform density of 0.239, while the outermost polymers form a shell which gets sharper with increasing Γ. Thus on increasing Γ, which may be due to the decrease in the temperature of the system or increase in the polymer charges, the polymers at the boundary would crystallize while the polymers at the center of the trap would still remain in a fluid state. Though the sharpness of the shells increases no new shells are formed. Unlike polymers, the density profile of point particles is monotonically decreasing and no shells are formed for any value of Γ. The differences between the two cases can be understood from the fact that the point particles do not have any internal structure and in the mean field limit we do not get any shells. For polymers even though the interpolymer correlations are neglected in the mean field, the stronger fluctuations within the polymer represented by $\omega(\mathbf{r})$ in Eq. (17) cause the formation of shells for longer polymers at couplings $\Gamma \sim 8$, as shown in Fig. 2(b). In other words, the shells appear for the longer polymers when the Coulomb or trap energy is approximately 8 times stronger the thermal energy. The plot clearly shows that for small polymers

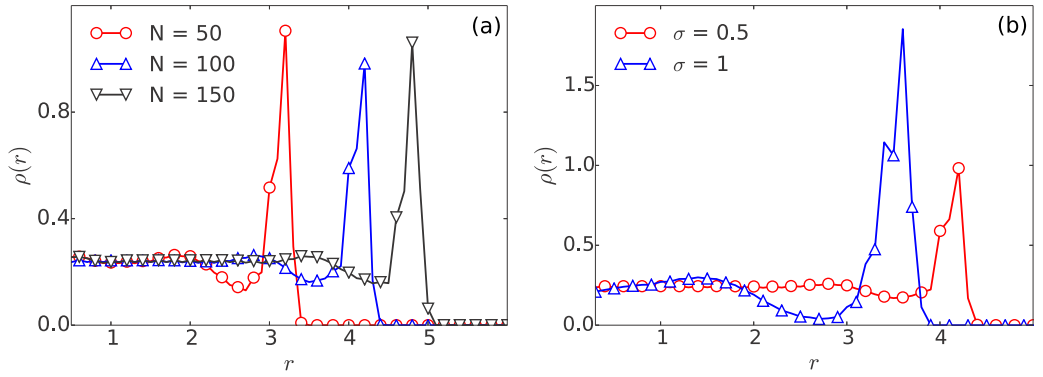

FIG. 3. Mean field. (a) Monomer densities for different values of the number of polymers in the trap N for $L = 8$ and $\sigma = 0.5$ at $\Gamma = 8$. Increasing N does not add any new shell. Instead the outermost shell moves outward. (b) Dependence of the monomer density on the monomer length σ of the polymers under the same conditions as in (a).

we recover the point-particle limit. Increasing the length of the polymers at a fixed $\Gamma = 8$ makes the outermost shell sharper; hence it is easier for them to crystallize. From Fig. 3(a) we see that on increasing the number of polyelectrolytes the outermost shell moves outward. The added polymers move to the inner fluid layer instead of populating the outermost shell or forming any new shells. Figure 3(b) depicts that thicker polymers or polymers with longer monomer lengths move inward because of having lower surface charge density and thus lower electrostatic repulsions. When either the electrostatic interactions or the trap is strong, the mean field approximation, which is valid at weak coupling strength, breaks down. In that case the interpolymer correlations play an important role in their shell structure and can no longer be neglected.

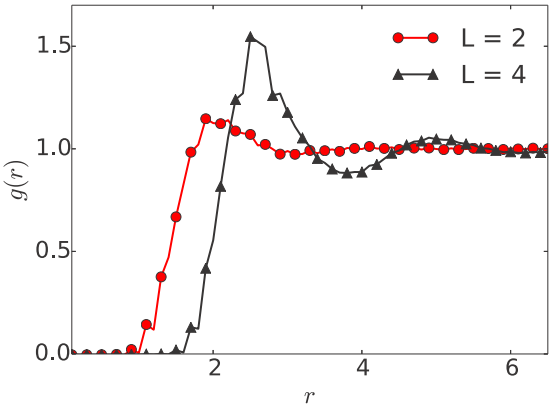

FIG. 4. Interpolymer pair correlation function for Gaussian polymers of lengths 2 and 4, respectively, $\Gamma = 4$ and $\sigma = 0.5$. The longer polymer shows peaks in $g(r)$ due to stronger correlations.

IV. GAUSSIAN POLYELECTROLYTES: BEYOND MEAN FIELD

In this section we explicitly consider the interpolymer correlations and study their effects on the shell structure of Gaussian polymers. We solve for the direct correlation function self-consistently from the LWC equation (12) and PRISM equation (13) by following the procedure outlined by Shew and Yethiraj [50]. The pair correlation functions in Fig. 4 clearly portray that the longer polymers are more strongly correlated, as seen from the peaks in the correlation functions. The direct correlation function is then plugged into Eq. (16) to obtain the effect potential $U(r)$ and from Eq. (15) the complete density profile. Again, Picard's algorithm is used to compute $U(r)$ in Eq. (16). The convergence of the numerical computations becomes increasingly slow for longer polymers and at large values of Γ. In that case mixing of different solutions produces faster convergence [49].

Figures 5(a) and 5(b) show that after taking into account the interpolymer correlations, sharp shells can occur at lower Γ or smaller lengths of the polymers. In Fig. 5(a) we see that on increasing the trap strength Γ the shells become sharper, the trend we obtained earlier in the mean field case. In the experiments and simulations on trapped colloidal systems, the strength of the trap is the primary controlling parameter. Increasing the strength of the trap leads to the formation of sharper shells [25,35,36]. Our observations from Fig. 5(a) qualitatively agree with these experimental and simulation results. As the shells become sharper and their overlap becomes zero, it becomes more and more difficult for the polymers to move from one shell to another. Thus the system is effectively frozen in the radial direction but is in a fluid phase within each shell, as concluded in Refs. [25,26,35]. At still higher Γ the system crystallizes and the liquid state theories are no longer valid.

Figure 5(b) shows that while the shorter polymers essentially behave like point particles with no shells at moderate Γ's, the longer polymers by virtue of being more strongly correlated produce sharp shells at such couplings. While in the mean field on increasing the number of polymers in the trap does not produce any new structure, for the correlated case the behavior is different. New shells appear as the number of polymers in the trap increases, as depicted in Fig. 6. The new shells start forming at the origin and the outermost shell moves outward to accommodate the newer ones, similar to the point-particle case [25]. For the point particles, however, the shells start forming at large $\Gamma \geqslant 10$ values [25], whereas for longer polymers the shells form as low as $\Gamma = 2$. Figure 6 also shows the dependence of the density structure on the diameter (or monomer length) of the polymers. For thicker polymers the

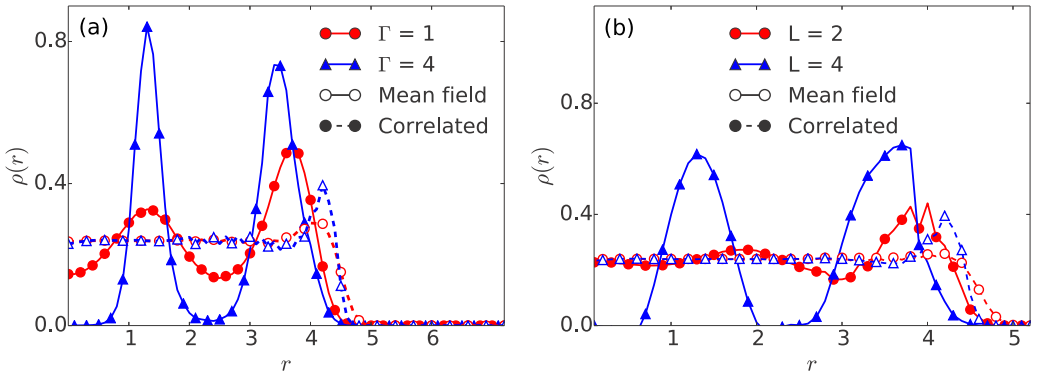

FIG. 5. Correlated densities. (a) The dependence of the correlated density profile (solid, filled) for 100 polymers with $L = 4$ on Γ. Also shown are the mean field density profiles (dashed, unfilled). Strong correlations at larger Γ produce sharper shells. (b) Correlated (solid) and mean field (dashed) monomer densities for different lengths L of the polymers at $\Gamma = 4$. Longer polymers are more strongly correlated and hence have sharper shells. All the polymers have the same $\sigma = 0.5$.

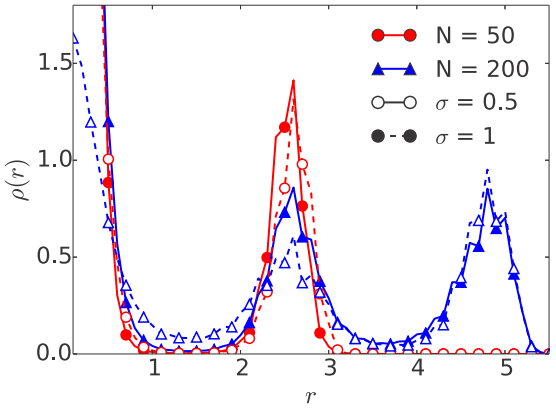

FIG. 6. Correlated densities. On increasing the number of polymers with $L = 4$ at $\Gamma = 4$ in the trap, new shells are formed unlike in the mean field case. Polymers of monomer lengths $\sigma = 0.5$ (solid, filled) and 1 (dashed, unfilled) are considered.

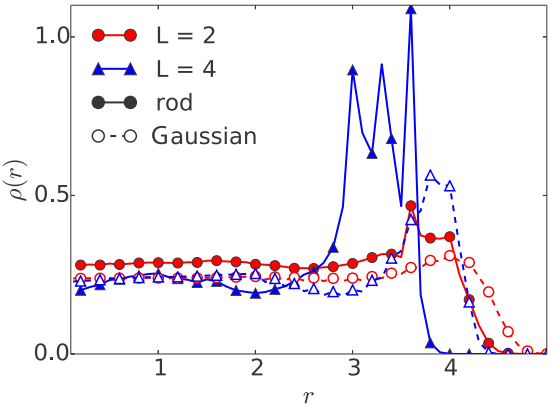

FIG. 7. Mean field. The monomer densities of 100 rodlike (solid) and Gaussian polymers (dashed) for different polymer lengths at $\Gamma = 4$. All the polymers have a monomer length of 1. The outermost shell is sharper for the rods than the Gaussian polymers. The three sharp peaks at the boundary are not individual shells but part of the outermost shell.

sharpness of the shells decreases slightly, although the effect of the variation of the polymer diameter is less pronounced after including the correlations.

V. RODLIKE POLYELECTROLYTES

In this section we look at rigid rodlike polymers, which is the opposite limit to the flexibility of the Gaussian polymers we studied in the earlier sections. For rodlike polymers the single chain structure factor $\hat{\omega}(\mathbf{k})$ in Eqs. (16) and (17) is given by [50]

$$\hat{\omega}(\mathbf{k}) = 1 + \frac{2}{L}\sum_{j=1}^{L-1}(L-j)\frac{\sin jk\sigma}{jk\sigma}. \tag{19}$$

The mean field densities for the rods show a sharper outermost shell than the Gaussian polymers in Fig. 7. This is due to the stronger correlations in the rods than the Gaussian polymers, which results in their having sharper outermost shells. Figures 8 and 9 on the correlated densities show that the shells of rodlike polymers are sharper and are shifted more outward than the Gaussian polymers. The rigidity causes strong repulsions among the rods compared to the Gaussian polymers, and they move outward to minimize the repulsions.

On changing the parameters Γ and L in Figs. 8(a) and 8(b), the rodlike polymers qualitatively behave in the same way as Gaussian chains. However, the correlated densities of rods in Fig. 9 have a strong dependence on the diameter of the rods (or monomer length) than the Gaussian polymers in Fig. 6. This is again due to the rigidity of the rods causing a decrease in the charge density due to the increase in the diameter (or monomer lengths), which has a stronger effect on the correlated densities.

VI. CONCLUSIONS AND DISCUSSIONS

We presented a theoretical description of polymer systems in an external potential. We have phenomenologically developed our theory for polymer systems in an external potential based on the RISM formalism of Chandler *et al.* [43,44] and have obtained an integral equation for the equilibrium density. Unlike most polymer field theoretic approaches where most of the computations are done in mean field, this theory goes beyond mean field and incorporates correlations though the LWC and PRISM formalisms. We have also looked at the specific case of the Gaussian and rodlike polymers trapped in a harmonic potential. In the small polymer limit we obtain the

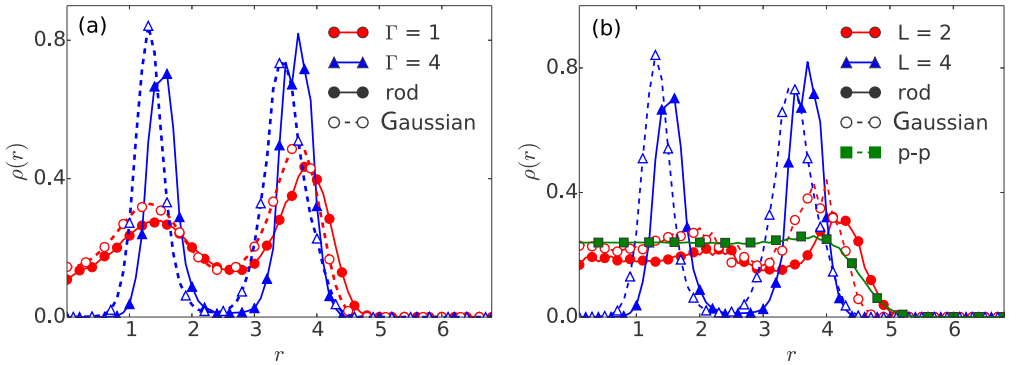

FIG. 8. Correlated densities. The density profile of 100 rodlike polymers (solid) and Gaussian polymers (dashed) for different values of (a) Γ's at $L = 4$ and (b) L's at $\Gamma = 4$. The shells move outward for rodlike polymers due to stronger electrostatic repulsions. All polymers have $\sigma = 0.5$.

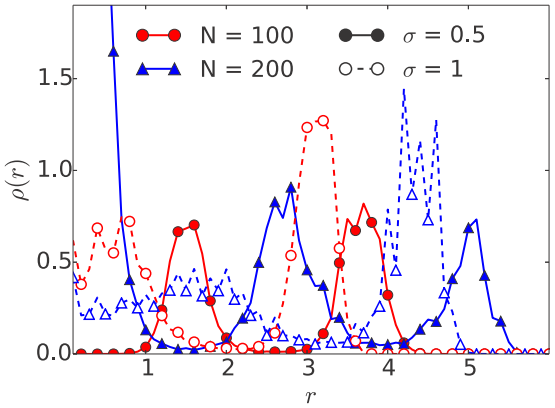

FIG. 9. Correlated densities. The density profile for rodlike polymers of length 4 at $\Gamma = 4$ showing more shells formed in the case of $N = 100$ and 200 polymers in the trap. Polymers of different monomer lengths $\sigma = 0.5$ (filled) and 1 (unfilled) are also considered. The density depends strongly on the diameter of the rods, unlike the Gaussian polymers in Fig. 6.

point-particle results of Wrighton [25]. The density profiles both in the mean field approximation and beyond mean field are explored for different models of the polymers and strengths of the trap potential. This work is effectively a generalization of the formalism developed by Wrighton *et al.* [25,26] for trapped point-charge to trapped polyelectrolyte systems.

This formalism would provide a useful description for the microstructures that form in polymer colloids confined in optical traps. In recent years structural transitions in trapped colloids as well as plasmas have attracted the attention of experimentalists as well as theorists [34–39]. The colloidal and dusty plasmas have been found to form shell structures in 3D and rings in 2D similar to the predictions by our model. At strong trap strengths we get sharp shells where the intershell transitions do not occur, while the polymers inside each shell remain in a fluid phase as was concluded in Refs. [35] and [36]. In most of these studies the presence of an attractive potential or multiple species causes the formation of additional structures. Including attractive interactions in our model would enable us to explain the self-assembly of trapped colloids and these new phases. The studies on structural transitions of colloidal systems in traps have considered spherical particles and are simpler than the biomolecules considered in our theory because of their complex geometries and additional length scales. Most experimental studies focus on the trapping of single molecules. Although trapping of multiple charged molecules can done through a technique called optical bottle [4,51], analysis of the pattern formations like the one in this work have not been done yet, to the best of the authors' knowledge. Simulations and experiments on the pattern formations in charged biomolecules would provide an important test for the many-body theories such as the one developed here.

Since the theory is based on the averaging over polymer sites for inhomogeneous polymer systems, it would describe the smaller polymers more accurately. For short polymers, however, the end effects become important and the averaging process would run into problems. The problem with the averaging related to the effects of the end points would not arise in ring polymers. For longer polymers the computations of the correlations become increasing difficult. The equation for the density has been derived through linearization, which would be valid for weak to moderate couplings. Simulations have to be performed to check the accuracy of the model at strong coupling. Most real life systems are better described by semiflexible polymers of which the Gaussian and the rodlike polymers are special cases. The semiflexible polymers, however, have an additional directional degree of freedom which adds to the complexity of the problems. We will tackle these problems in a subsequent paper.

ACKNOWLEDGMENT

This research was supported by Basic Science Research Program through the National Research Foundation of Korea (NRF) funded by the Ministry of Education (Grants No. NRF2015R1D1A1A09061345 and No. NRFC1ABA00120110029960).

[1] S. Weiss, Science **283**, 1676 (1999).
[2] S. Fujii, K. Kanaizuka, S. Toyabe, K. Kobayashi, E. Muneyuki, and M.-A. Haga, Langmuir **27**, 8605 (2011).
[3] J. Fu and H. D. Ou-Yang, in *SPIE NanoScience + Engineering* (International Society for Optics and Photonics, Bellingham, WA, 2014), pp. 91641V–91641V.
[4] S. Park, S. Q. Choi, C. Song, M. W. Kim, and M. C. Choi, Soft Matter **10**, 8406 (2014).
[5] S.-H. Kim, S. Y. Lee, S.-M. Yang, and G.-R. Yi, NPG Asia Materials **3**, 25 (2011).
[6] H. Yoshikawa, S. Imura, and E. Tamiya, Anal. Chem. **84**, 9811 (2012).
[7] Y. Nabetani, H. Yoshikawa, A. C. Grimsdale, K. Müllen, and H. Masuhara, Langmuir **23**, 6725 (2007).
[8] Z. Nie and E. Kumacheva, Nature Mater. **7**, 277 (2008).
[9] J. Zhang, Z. Sun, and B. Yang, Curr. Opin. Colloid Interface Sci. **14**, 103 (2009).
[10] V. Boyer, R. M. Godun, G. Smirne, D. Cassettari, C. M. Chandrashekar, A. B. Deb, Z. J. Laczik, and C. J. Foot, Phys. Rev. A **73**, 031402 (2006).
[11] F. M. Fazal and S. M. Block, Nat. Photonics **5**, 318 (2011).
[12] J. Xavier, R. Dasgupta, S. Ahlawat, J. Joseph, and P. K. Gupta, Appl. Phys. Lett. **101**, 201101 (2012).
[13] S. Ito, H. Yoshikawa, and H. Masuhara, Appl. Phys. Lett. **78**, 2566 (2001).
[14] M. Toshimitsu, Y. Matsumura, T. Shoji, N. Kitamura, M. Takase, K. Murakoshi, H. Yamauchi, S. Ito, H. Miyasaka, A. Nobuhiro *et al.*, J. Phys. Chem. C **116**, 14610 (2012).
[15] T. Shoji, J. Saitoh, N. Kitamura, F. Nagasawa, K. Murakoshi, H. Yamauchi, S. Ito, H. Miyasaka, H. Ishihara, and Y. Tsuboi, J. Am. Chem. Soc. **135**, 6643 (2013).

[16] N. Murazawa, S. Juodkazis, and H. Misawa, Eur. Phys. J. E **20**, 435 (2006).
[17] E. Brasselet, N. Murazawa, S. Juodkazis, and H. Misawa, Phys. Rev. E **77**, 041704 (2008).
[18] J. Jeong, Z. S. Davidson, P. J. Collings, T. C. Lubensky, and A. Yodh, Proc. Natl. Acad. Sci. USA **111**, 1742 (2014).
[19] J. Jeong, L. Kang, Z. S. Davidson, P. J. Collings, T. C. Lubensky, and A. Yodh, Proc. Natl. Acad. Sci. USA **112**, E1837 (2015).
[20] M. Drewsen, C. Brodersen, L. Hornekær, J. S. Hangst, and J. P. Schifffer, Phys. Rev. Lett. **81**, 2878 (1998).
[21] O. Arp, D. Block, A. Piel, and A. Melzer, Phys. Rev. Lett. **93**, 165004 (2004).
[22] M. Bonitz, D. Block, O. Arp, V. Golubnychiy, H. Baumgartner, P. Ludwig, A. Piel, and A. Filinov, Phys. Rev. Lett. **96**, 075001 (2006).
[23] O. Arp, D. Block, M. Klindworth, and A. Piel, Phys. Plasmas **12**, 122102 (2005).
[24] S. Juodkazis, N. Mukai, R. Wakaki, A. Yamaguchi, S. Matsuo, and H. Misawa, Nature (London) **408**, 178 (2000).
[25] J. Wrighton, J. W. Dufty, H. Kählert, and M. Bonitz, Phys. Rev. E **80**, 066405 (2009).
[26] H. Bruhn, H. Kählert, T. Ott, M. Bonitz, J. Wrighton, and J. W. Dufty, Phys. Rev. E **84**, 046407 (2011).
[27] J. Wrighton, J. Dufty, M. Bonitz, and H. Kählert, Contrib. Plasma Phys. **50**, 26 (2010).
[28] A. A. Koulakov and B. I. Shklovskii, Phys. Rev. B **57**, 2352 (1998).
[29] V. M. Bedanov and F. M. Peeters, Phys. Rev. B **49**, 2667 (1994).
[30] M. Kong, B. Partoens, and F. Peeters, New J. Phys. **5**, 23 (2003).
[31] J. A. Drocco, C. J. Olson Reichhardt, C. Reichhardt, and B. Janko, Phys. Rev. E **68**, 060401 (2003).
[32] S. W. W. Apolinario, B. Partoens, and F. M. Peeters, Phys. Rev. B **77**, 035321 (2008).
[33] V. A. Schweigert and F. M. Peeters, Phys. Rev. B **51**, 7700 (1995).
[34] Y. Liu, Z. Chen, F. Huang, M. Yu, L. Wang, and A. Bogaerts, Phys. Plasmas **13**, 052110 (2006).
[35] E. C. Euán-Díaz, S. Herrera-Velarde, V. R. Misko, F. M. Peeters, and R. Castañeda-Priego, J. Chem. Phys **142**, 024902 (2015).
[36] S. A. Rice, Chem. Phys. Lett. **479**, 1 (2009).
[37] L. Q. Costa Campos, S. W. S. Apolinario, and H. Löwen, Phys. Rev. E **88**, 042313 (2013).
[38] K. Nelissen, B. Partoens, and F. M. Peeters, Phys. Rev. E **71**, 066204 (2005).
[39] Y. H. Liu, L. Y. Chew, and M. Y. Yu, Phys. Rev. E **78**, 066405 (2008).
[40] F. Evers, R. D. L. Hanes, C. Zunke, R. F. Capellmann, J. Bewerunge, C. Dalle-Ferrier, M. C. Jenkins, I. Ladadwa, A. Heuer, R. Castañeda-Priego *et al.*, The European Physical Journal Special Topics **222**, 2995 (2013).
[41] E.-L. Florin, A. Pralle, E. Stelzer, and J. Hörber, Appl. Phys. A: Mater. Sci. Process. **66**, S75 (1998).
[42] Y. Roichman, B. Sun, A. Stolarski, and D. G. Grier, Phys. Rev. Lett. **101**, 128301 (2008).
[43] D. Chandler, J. D. McCoy, and S. J. Singer, J. Chem. Phys **85**, 5971 (1986).
[44] D. Chandler, J. D. McCoy, and S. J. Singer, J. Chem. Phys **85**, 5977 (1986).
[45] J. G. Curro and K. S. Schweizer, Macromolecules **20**, 1928 (1987).
[46] K. S. Schweizer and J. G. Curro, Phys. Rev. Lett. **58**, 246 (1987).
[47] K. Schweizer and J. Curro, in *Atomistic Modeling of Physical Properties* (Springer, Berlin, 1994), pp. 319–377.
[48] D. Laria, D. Wu, and D. Chandler, J. Chem. Phys **95**, 4444 (1991).
[49] J.-P. Hansen and I. R. McDonald, *Theory of Simple Liquids* (Elsevier, New York, 1990).
[50] C.-Y. Shew and A. Yethiraj, J. Chem. Phys. **106**, 5706 (1997).
[51] J. Junio, S. Park, M.-W. Kim, and H. D. Ou-Yang, Solid State Commun. **150**, 1003 (2010).